JOURNAL OF GEOPHYSICAL RESEARCH, VOL. 113, F01003, doi:10.1029/2007JF000753, 2008

Experiments on the non-Boussinesq flow of self-igniting suspension currents on a steep open slope

B. Turnbull[1,2,3] and J. N. McElwaine[2]

Received 12 January 2007; revised 20 August 2007; accepted 27 September 2007; published 19 January 2008.

[1] Pyroclastic flows from volcanoes, dust storms in the desert, and submarine turbidity currents are all gravity currents of particles in suspension occurring in nature. Powder snow avalanches are one such flow where the density difference between the suspended particles and the interstitial air is high and the particles carry a significant proportion of the flow's momentum. This means that the Boussinesq approximation, where density differences are considered negligible in inertia terms, is not valid. Aspects of such flows, such as their internal structure and the transition from a dense flow to a suspension current are not well understood. Repeatable laboratory experiments are necessary for a better understanding of the underlying physics. Up to now, an experiment has not been designed with the correct similarity criteria for modeling powder snow avalanches. We have addressed this by designing and analyzing the results from a new experimental model of powder snow avalanches that had three distinctive features. Fine, dry snow was used to form suspension currents in air. The high density ratio of powder snow avalanches was preserved so that the currents are non-Boussinesq. Our experiments started with a dense current that then self-ignited, undergoing the transition to a suspension current. The shape and position of the current was tracked with two video cameras, and the air flow measured with a high-frequency response pressure transducer mounted in the base. We show how the air pressure data closely match theory and reveal whether a current is primarily dense or suspended.

Citation: Turnbull, B., and J. N. McElwaine (2008), Experiments on the non-Boussinesq flow of self-igniting suspension currents on a steep open slope, *J. Geophys. Res.*, *113*, F01003, doi:10.1029/2007JF000753.

1. Introduction

[2] Powder snow avalanches are avalanches where some of the snow is suspended by the air forming a powder cloud. This powder cloud flows as a gravity currents driven by the density difference between the particle suspension and the surrounding ambient air [*Simpson*, 1997]. Powder snow avalanches usually start as a dense granular flow of snow down a slope. As the material accelerates down the slope, turbulent eddies in the ambient air entrain particles from the upper surface and front, in a manner similar to the saltation of snow particles by wind to form snow drifts [*Parker et al.*, 1986; *Issler*, 1998]. If sufficient material becomes suspended and the turbulence is sufficient to maintain the excess density, the suspended powder cloud can flow down the slope as a gravity current. These are the conditions for self-ignition [*Parker*, 1982]. In natural powder snow avalanches the transition mechanism is usually very rapid, because the flows are strongly accelerating over the period of transition so that suspension occurs at rates much higher than the settling velocity. Thus the saltation, or partly suspended phase is brief. Our experiments however, and the ping-pong ball avalanches [*Nishimura et al.*, 1998; *McElwaine and Nishimura*, 2001], occur very close to the transition point so that the saltation-suspension mechanism is less explosive and partly suspended currents, where a saltation type layer exists, are longer-lived.

[3] In the early stages, while a snow avalanche accelerates, the dynamics of the powder cloud and the dense granular avalanche, from which it initiated, are strongly coupled. As the turbulence within the powder cloud increases and the suspension becomes self-sustaining, video and radar measurements show that its front is usually ahead of the dense granular avalanche [*Dufour et al.*, 1999, 2000, 2001, 2002, 2003, 2004, 2005]. Although the dense granular avalanche typically erodes snow cover that is then entrained into the powder cloud, the dynamics of the two parts are distinct. Powder clouds have been observed to follow different routes to their dense granular counterparts, and they may continue for significant distances after the dense avalanche has stopped [*Margreth*, 2000]. In this work we use the term powder snow avalanche to describe any

[1] Wald, Schnee und Landschaft, Swiss Federal Institute of Snow and Avalanche Research, Davos Dorf, Switzerland.
[2] Department of Applied Mathematics and Theoretical Physics, University of Cambridge, Cambridge, UK.
[3] Now at Mechanical and Aerospace Engineering, Cornell University, Ithaca, New York, USA.

0148-0227/08/2007JF000753$09.00

avalanche where a "powder cloud" forms, and we define a powder cloud as a snow-air suspension at low volume concentrations where direct particle-particle forces are negligible. This is in contrast to the dense layer at the base of an avalanche where motion of the air has a negligible effect compared with intergranular collisions.

[4] Field measurements from powder snow avalanches are becoming more successful and increasingly more information about the internal dynamics is available [*Turnbull et al.*, 2007; *Turnbull and McElwaine*, 2007]. However, serious problems remain with field experiments. They are expensive to run owing to the cost of material, logistics and damage caused by both the avalanches being measured and the harsh weather conditions in the places where the avalanches occur. The data can be difficult to interpret and the experiments are impossible to reproduce because of the lack of control in the boundary and initial conditions. These factors make the main physical processes in avalanches difficult to identify with field measurements. Laboratory experiments are needed to test theories and to investigate the key processes, an essential step before complete models of mixed avalanche motion can be developed. With these scaled experiments, repeatable suspension currents (i.e., gravity currents where the driving density difference arises as a result of particles suspended in the ambient fluid) of snow in air are generated from a dense granular flow.

[5] Most previous experiments of particulate gravity currents use water as the ambient fluid [*Hermann et al.*, 1987; *Beghin and Olagne*, 1991]. For such experiments the density ratio between the current and the ambient fluid is very low, usually a few percent, and those currents are in the Boussinesq regime. This means that the particles' momentum is very small relative to that of the interstitial fluid, significantly affecting the dynamics and mixing in the current (2). *Hampton* [1972] and *Ancey* [2004] used very concentrated suspensions in water to generate density differences approaching the non-Boussinesq case, but these are still an order of magnitude lower than the density differences found in powder clouds.

[6] Additionally, few experiments have considered the transition from a dense flow to a suspension current. In the previous experiments of *Assier Rzadkiewicz et al.* [1997] and *Hampton* [1972], some grains from debris flows of clay or sand slurries entered suspension by entraining ambient water to form turbidity currents. In general, experimental models of powder clouds [*Hermann et al.*, 1987; *Beghin and Olagne*, 1991] have so far avoided modeling this transition between a dense flow and a suspension current. These experiments use a dense ambient fluid or a premixed turbulent suspension to model the dynamics of developed suspension currents, but they do not attempt to model the saltation and suspension mechanisms.

[7] One exception [*Bozhinskiy and Sukhanov*, 1998] used very fine (0.1 mm and 0.01 mm respectively) sawdust and aluminum particles, but for such fine particles the interaction with the air is through viscous drag forces and is not the same as for much larger snow crystals. Other experiments using ping-pong balls [*Nishimura et al.*, 1998; *McElwaine and Nishimura*, 2001] on a ski jump have shown a saltation layer on top of a dense granular flow, but the transition to suspension was incomplete. As with field measurements from snow avalanches, such large-scale experiments are expensive and difficult to perform in a repeatable manner.

[8] With these laboratory experiments, varying degrees of suspension are achieved by varying the slope angle of the chute. For shallow angles few particles enter suspension and the current remains a dense granular flow. With a vertical chute, the particles are entirely suspended and the current behaves like a plume. At some intermediate angle, it is possible to have just enough particles entering suspension that they start to flow as a suspension current. In this way the mechanism by which snow particles can form a powder cloud is replicated.

[9] The primary motive of this experiment is to investigate flows of dry, fine snow. This is difficult because snow sinters and metamorphoses in a few minutes. The practical difficulties in generating repeatable snow currents mean it is useful to compare the snow currents with currents of polystyrene balls, which have far better controlled initial conditions. Air pressure and video data from both snow and polystyrene currents are analyzed in detail to draw conclusions about the internal structure of non-Boussinesq, particle-driven gravity currents on an incline. In the following section, similarity criteria for both the snow and polystyrene currents are discussed in the context of previous experiments.

2. Similarity Criteria

[10] The chute experiments not only model the transition between different flow regimes, but also the similarity criteria appropriate for the formation of powder clouds in avalanches. Table 1 summarizes a range of experiments on suspension currents in terms of the relevant dimensionless numbers that characterize them. These numbers are introduced and discussed in this section

[11] For all of the experiments listed in Table 1 the Reynolds number of the flow, which determines the degree of turbulence in the flow, is significantly lower than the Reynolds number for a powder snow avalanche (the ping-pong ball avalanches of *Nishimura et al.* [1998] and *McElwaine and Nishimura* [2001] provide the closest similitude). However all of the experimental flows have Reynolds numbers within a turbulent regime, which we would expect to provide similar flow characteristics to natural powder snow avalanches.

[12] The bulk Richardson number (hereafter referred to as the Richardson number, Ri) determines whether a sheared interface between two fluids is stable or unstable [*Ellison and Turner*, 1959]. It can be thought of as the ratio of potential energy to kinetic energy of a parcel of the dense particles at the interface if they move up in to the ambient fluid. For a layer of height h and velocity u on a slope at angle θ to the horizontal, the Richardson number for the layer is

$$\mathrm{Ri} = \frac{g' h \cos\theta}{u^2}. \tag{1}$$

The reduced gravity is $g' = g\Delta\rho/\rho_a$, where $\Delta\rho = \rho - \rho_a$ with ρ and ρ_a the densities of the current and the ambient fluid respectively. A dense flow will entrain air on the upper surface and become suspended if the Richardson number is

Table 1. Magnitudes of Five Dimensionless Numbers That Characterize Suspension Current Experiments[a]

Experiment	Materials	Re_p	Ri	St	$\frac{\Delta\rho}{\rho_a}$	Re
Powder snow avalanches *Turnbull et al.* [2007]	**snow-air**	**3000**	**1**	**0.02**	**10**	$\mathbf{10^9}$
Ancey [2004]	sawdust/sand suspension-water	50	1.7	0.006	0.05	10^4
Bozhinskiy and Sukhanov [1998]	sawdust and aluminum mixture-air	0.1	20	0.03	1	10^3
Beghin et al. [1981], *Beghin and Brugnot* [1983], and *Beghin and Olagne* [1991]	brine-water/sand-water suspension	-	5	-	0.02	10^4
Nishimura et al. [1998] and *McElwaine and Nishimura* [2001]	ping-pong balls-air	2×10^4	2	10	50	10^7
Hampton [1972]	kaolinite and water slurry	-	<0.5	-	0.1	-
Hermann et al. [1987]	polystyrene powder-water	1.5	0.1	1×10^{-4}	0.002	10^4
Hopfinger and Tochon-Danguy [1977] and *Tochon-Danguy and Hopfinger* [1974]	brine-water	-	2	-	0.01	10^3
Present study	**snow-air**	**150**	**1**	**10**	**10**	$\mathbf{10^5}$
Present study	**polystyrene-air**	**150**	**2**	**1**	**5**	$\mathbf{10^4}$

[a]Particle Reynolds number, Re_p; Richardson number, Ri; Stokes number, St; density ratio, $\frac{\Delta\rho}{\rho_a}$; and Reynolds number, Re. The similarity criteria for previous experiments are compared with those for powder snow avalanches and with those for the snow currents and the polystyrene currents in the present study.

low enough, and subsequently the suspension current will maintain the particles in suspension and further entrain air if the Richardson number stays low enough. Thus the value of Ri provides an indication of the stability of the flow. It can be useful to consider Ri as the inverse of the square of the densimetric Froude number. A local gradient Ri can also be defined in a continuous stratification and linear stability analysis of a stratified shear flow shows that the flow is unstable to two-dimensional disturbance if the gradient Ri < $\frac{1}{4}$ [*Turner*, 1973].

[13] Previous experiments modeling powder clouds [*Beghin et al.*, 1981; *Beghin and Olagne*, 1991] are characterized by values of Ri of order 5 (Table 1) and the interface is relatively stable. Over most of its lifetime a powder snow avalanche typically has values of Ri less than 1, where the interface will be locally unstable [*Simpson*, 1997], and consequently there is a higher entrainment rate of ambient fluid compared with Beghin's work. In the early stages of powder snow avalanche motion Ri is greater than 1 and Beghin's experiments provide a closer match. However, these elevated values of Ri in a developing powder snow avalanche are due to the high density ratios and low velocities, whereas the *Beghin et al.* [1981] and *Beghin and Olagne* [1991] experiments were carried out in water resulting in very low density ratios and thus elevated Ri. In the present experiments, to both preserve the particle-ambient density ratio for powder snow avalanches by making chute flows of snow particles in air, and keep a low Ri, very steep slope angles are needed. Thus, for the snow in air experiments, the slope angle is varied between 40° and 90°.

[14] In the snow-air experiments, a very high particle-ambient density ratio (≈ 1000) is preserved compared with most experiments, which use a denser ambient fluid such as water. Both natural powder snow avalanches and the snow-air experimental currents are non-Boussinesq, where density differences are important in both dynamic and buoyancy terms [*Boussinesq*, 1903]. This contrasts with experiments where a dense ambient fluid is used, and the currents are in the Boussinesq regime. In a snow-air suspension current, the relatively heavy snow particles carry a significant proportion of the current's momentum. For suspension currents with a relatively low density ratio, for example saw dust-water currents, the inertia of the particles is small compared with the inertia of the ambient fluid. *Hampton* [1972] and *Ancey* [2004] achieved density differences that approach the non-Boussinesq case by using high-concentration suspensions in water.

[15] The experiments of *Hermann et al.* [1987], with fine polystyrene powder in water, obtain realistic values of Ri by using a very low density ratio, $\Delta\rho/\rho_a \approx 0.002$ (Table 1). Although the mixing processes in these polystyrene powder-water currents will be similar to the mixing in powder snow avalanches, the relatively high level of momentum carried by the particles in a powder snow avalanche will not be well modeled in the *Hermann et al.* [1987] experiments.

[16] There are two possible drag regimes for a particle of diameter d_p, mass m and with a velocity relative to the interstitial fluid that is proportional to the absolute velocity u. In a viscous regime the drag varies linearly with velocity and has an associated timescale [*Batchelor*, 1967]

$$\tau_1 = \frac{m}{d_p \mu}, \tag{2}$$

for an ambient fluid of viscosity μ. For higher speeds, the drag is dominated by pressure forces resulting in form drag and varies quadratically with velocity. In this case the associated timescale is

$$\tau_2 = \frac{m}{\rho_a d_p^2 u}, \tag{3}$$

where ρ_a is the ambient fluid density.

[17] The ratio of the viscous and form drag timescales is

$$\frac{\tau_1}{\tau_2} = \frac{\rho_a u d_p}{\mu}, \tag{4}$$

which is the particle Reynolds number, Re_p, of the flow. The particle Reynolds number determines whether the drag is dominated by viscous or pressure forces. For experiments such as those by *Bozhinskiy and Sukhanov* [1998] and

Hermann et al. [1987] the particle Reynolds number is very low ($\ll$10) as a result of using very fine particles. With very small particles and a low Re_p, the drag force exerted on the particles from the ambient fluid is almost entirely through viscous forces. For a powder snow avalanche Re_p is several orders of magnitude larger and viscous drag forces play a relatively minor role compared to the form drag of the particle. The ping-pong ball experiments [*Nishimura et al.*, 1998] modeled the interaction between snow particles and ambient air relatively well with a very high particle Reynolds number $\mathrm{Re}_p \approx 2 \times 10^4$ (compared with 3000 for powder snow avalanches). For values $500 < \mathrm{Re}_p < 10^5$, the regime for powder snow avalanches, the drag coefficient for a spherical particle is essentially independent of Re_p [*Batchelor*, 1967]. This means that within this range of Re_p, the particle ambient interaction in powder snow avalanches will be well modeled.

[18] The chute experiments of snow in air will have identical values of $\rho_a \approx 1$ kg m^{-3}, $d_p \approx 10^{-3}$ m and $\mu \approx 1.7 \times 10^{-5}$ Pa s as powder snow avalanches. By releasing only a finite volume of snow, and given the short length of chute relative to an avalanche track, the chute currents will reach much lower speeds than real powder snow avalanches. On the chute u_p is approximately 2 m s^{-1}, and the particle Reynolds number can be found from equation (4): $\mathrm{Re}_p \approx 1 \times 2 \times 10^{-3}/1.7 \times 10^{-5} \approx 150$. In comparison, powder snow avalanches have velocities $u_p = 50$ m s^{-1} and $\mathrm{Re}_p \approx 1 \times 50 \times 10^{-3}/1.7 \times 10^{-5} \approx 3000$. For the chute flows, viscous forces between the air and the snow particles will have a greater effect than in a powder snow avalanche. However, Re_p is still large enough for the chute flows that the viscous drag forces can be considered small.

[19] The Stokes number is used as a measure of the interplay between the particles and the fluid and the degree to which the suspension behaves as a two phase or a single phase flow [*Ancey*, 2007]. This depends on the drag regime and is defined in terms of the particle drag timescale τ and timescale of the flow h/u

$$\mathrm{St} = \frac{\tau u}{h}. \tag{5}$$

Thus for the viscous drag regime (where $\tau = \tau_1$, equation (2)) and form drag regime (where $\tau = \tau_2$, equation (3)) we have Stokes numbers

$$\mathrm{St}_1 = \frac{\rho_p u}{\mu}\frac{d_p^2}{h} \quad , \quad \mathrm{St}_2 = \frac{\rho_p d_p}{\rho_a h}, \tag{6}$$

respectively, where $m = \rho_p d_p^3$.

[20] With high values of Stokes number, the drag is weak and the particle is unaffected by fast variations in the fluid velocity. Thus the particle and fluid have a weak interplay and the suspension has strong multiphase character. For very low values of Stokes number, there are strong drag forces and the characteristic timescale of the flow is large. The motion of particles and fluid is strongly linked and the suspension behaves as a single phase [*Ancey*, 2007; *Batchelor*, 1989]. If the air in a powder snow avalanche is replaced by water in an experimental model, the fluid viscosity is increased many times leading to a reduction in St. Likewise if much finer or less dense particles than snow are used St is reduced, and the coupling between the solid and fluid phases is no longer appropriate for modeling powder snow avalanches. In our experiments with snow the Stokes number is large compared with powder snow avalanches because the flow is so much smaller. The polystyrene ball currents give more accurate Stokes number similarity and will provide an interesting contrast with the snow-air currents.

[21] Four dimensionless numbers (Ri, Re_p, St, and $\Delta\rho/\rho_a$) characterize the experiments. Other significant groups can be formed from the four given here, including the Reynolds number and the Shields parameter, which determines any entrainment at the bottom surface of a suspension. The inverse Shields parameter is proportional to Richardson number for an eroding suspension current.

[22] One further consideration is the sedimentation velocity of a particle normal to the slope, v_t. A length scale can be found

$$L = \frac{v_t^2}{g},$$

which determines the size of the experiment. In order to maintain a suspension the vertical fluctuations in the flow velocity must be the same order of magnitude as the settling velocity. For turbulent fluctuations 10% of the flow velocity, suspension will be maintained if $u > 10v_t$. For suspension to be maintained over the length of the chute, the chute length must be much greater than the length scale L. However the sedimentation velocity is not independent, since the length scale L is a function of the drag timescales given in equations (2) and (3). The terminal velocity is thus related to the particle Reynolds and Stokes numbers. The slope normal setting velocity is

$$v_t \propto \sqrt{g\tau_1 u \cos\theta} \quad \text{or} \quad v_t \propto \sqrt{g\tau_2 u \cos\theta}$$

respectively for viscous and form drag regimes and L is proportional to $\tau_1 u$ or $\tau_2 u$.

[23] One drawback of the small-scale snow-air experiments is that the ratio of the particles' settling velocity, v_t, to the velocity of the flow front, u_f, is very much higher in the snow-air experiments than in field powder snow avalanches since typical front velocities are 2m s^{-1} for the snow-air experiments compared with 50m s^{-1} for powder snow avalanches. Particle sedimentation on the upper surface of the laboratory snow-air currents is significant, though the currents will still resemble the early, initiation stages of a powder snow avalanche.

[24] Our experiments attempt to maintain similarity of Ri and $\Delta\rho/\rho_a$ to accurately model entrainment effects and the transition to suspension. The other parameters, Re, Re_p and *St*, are not matched exactly but they are within a range where the same flow behavior and dynamics are expected.

3. Experiment

[25] Over the winter 2002–2003 a simple experiment was designed and carried out where the transition between a dense flow of snow in air and a powder cloud could be studied. A 2-m wide, 3-m long, flat wooden chute with one

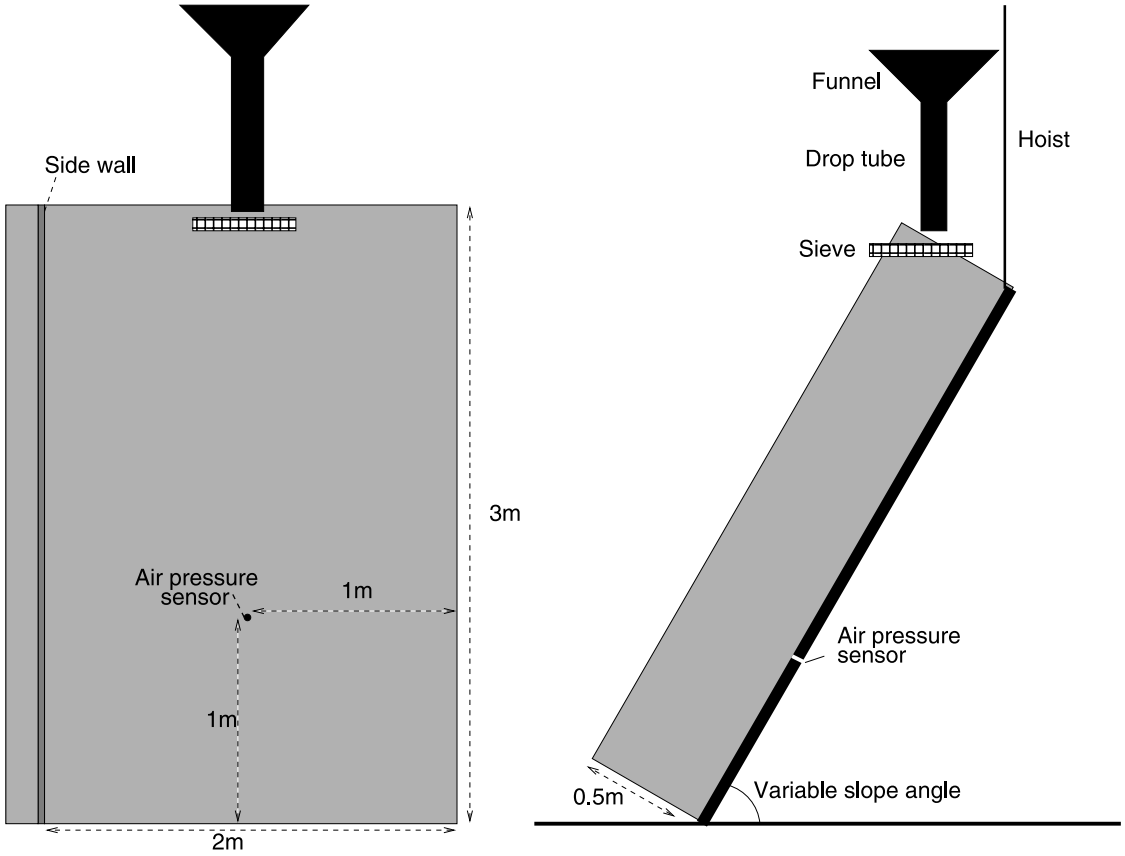

Figure 1. Configuration of an experiment investigating the flow of dry, natural snow on an inclined plane.

0.5-m-high side wall was installed in a cold, concrete bunker in the Flüelatal (1650 m a. s. l.) near Davos, Switzerland. The bottom was fixed with hinges to a frame and the top was attached to a hoist so that the chute could be inclined at any slope angle between 50° and vertical.

[26] Stationary, dry snow sinters into clumps in a few seconds, even at low temperatures. A significant difficulty to overcome with these experiments was to break the sintered bonds between snow grains and to start the snow flowing before resintering could occur. Initially, a fan in a release box was used to agitate the snow, similar to a fluidized bed [*Nishimura*, 1990]. However we were unable to maintain the snow in a noncohesive state and, after some experimentation, we abandoned this fluidization method and a different approach was adopted. The snow was dropped through a funnel into a 1-m-long drop-tube where it hit a sieve (mesh ≈10 mm), shown in Figure 1. The sieve broke the sintered bonds between snow grains and the powdered snow dropped onto the chute, down which it flowed. Any snow sticking to the sieve and funnel was removed after each experiment.

[27] The snow used was powder snow collected from the Weissfluhjoch (2663 m a. s. l., near Davos) directly after it fell, and stored in a cold room at −20° C until it was needed. By the time the snow was used, it had metamorphosed to be mostly round grained snow with grain sizes in the range 0.2 mm to 2 mm and a bulk density of around 200 kg m^{-3}, typical for cold room snow. Experiments were carried out for chute angles in steps of roughly 5°, between 50° and 87°. Around 20 currents of varying sizes were released at each slope angle.

[28] This successful system was not developed until April 2003 when ambient temperatures were close to zero. To prevent the snow from melting or sintering, it was necessary to carry the snow from the cold room and perform the experiments as quickly as possible. Each series of experiments (one series for each slope angle) was carried out in around 15 minutes over which time the snow properties and temperature did not change significantly. However this time constraint meant that measuring the release volumes was not possible, nor careful variation in the initial conditions.

[29] For comparison, and to assess the effects of the initial conditions, the experiments were repeated using 2–4 mm diameter polystyrene balls. The particles are noncohesive which simplifies the experiment. A sieve, which prevents sintering between the snow grains, is unnecessary for the polystyrene balls, resulting in more repeatable flow onto the chute. Without the time constraint imposed by the sintering snow, it was possible to measure the release volume of particles. Depending on the environmental conditions, static electricity can induce cohesion between polystyrene balls, but this effect was not observed during the experiments.

3.1. Video Measurements

[30] Two digital video cameras were placed to the side and in front of the chute so the flow surface could be reconstructed in three dimensions. The frontal camera was

Figure 2. Front view and side view stills from a 2l polystyrene ball current on a 70° open slope. For clarity, the images are deinterlaced and use an inverted color scheme with the background removed.

positioned as close as possible above and in the plane of the chute. The side camera was tilted so that the direction of flow was horizontal in the field of the camera, maximizing resolution. To give a good contrast between the snow flow and chute, the chute was painted matt black. White camera calibration dots were placed on the chute and supporting structure and their positions in three dimensions measured. They were arranged so that several were visible from each camera view.

[31] By identifying the calibration points in each video clip, parameters for camera properties such as focal length, position, rotation and lens distortion could be found. Knowing the precise set up and location of the camera, pixel coordinates on the video clips can be converted to three-dimensional, spatial locations. The videos were processed using a change-point method developed for granular flows [*McElwaine*, 2001]. This detects the arrival time of the flow at each pixel on the camera. Contours of this set of arrival times then correspond to the edge of the flow at a particular time. Front position, velocity and flow height data can be calculated from these contours.

3.2. Air Pressure Measurements

[32] The dynamics and structure of flows with such high Reynolds numbers as powder snow avalanches are determined by their interaction with the ambient air. There are air pressure measurements available from large natural snow avalanches [*Nishimura et al.*, 1995; *Turnbull et al.*, 2007] as well as ping-pong ball experiments [*McElwaine and Nishimura*, 2001], so they are a particularly useful measurement to make to allow comparison across size scales. A Validyne DP103 pressure sensor with a range of 0 to 35 Pa, was installed in the chute surface in the center of the chute 1 m from the bottom edge, marked on Figure 1, to measure the air flow in front of and inside the currents. The sensor was connected using a very short tube ($\approx$ 20 mm) to maximize the frequency response which was tested by applying step changes in pressure using a bicycle pump. The lowest resonance frequency response was found to be better than 200 Hz.

4. Results

[33] Stills from the front view and side view videos of a 2 l polystyrene ball current on a 70° slope are shown in Figure 2. The original images have been deinterlaced and processed to remove the background. By inverting the color scheme, so that the polystyrene balls appear black rather than white, the flow structures can be seen more clearly. It is simpler to see the flow structures inside the polystyrene ball currents than the snow currents, since the polystyrene balls are larger and thus reflect light more effectively than the snow particles. Denser regions of flow reflect more light than less dense regions. This means that in the inverted images, denser regions appear darker than less dense regions.

[34] From the front view of the polystyrene ball current in Figure 2, a dense crescent-shaped head with a tail along the flow axis can be seen. These are typical characteristics of granular flows [*Nishimura et al.*, 1998; *McElwaine and Nishimura*, 2001]. A faster flowing, dense tail feeds material into the head, where drag from the particles' interaction with the ambient fluid causes the nose to roll up into the crescent shape. The dense regions in the head and tail can also be seen from the side view of the polystyrene ball current in Figure 2. The head rolls up to give a dense nose with a region of less dense recirculation behind the head. The nose of the current is slightly raised from the chute surface. This effect is due to friction at the surface, observed for a range of gravity current experiments [*Simpson*, 1997; *Britter and Linden*, 1980; *Beghin et al.*, 1981].

[35] Similar structures to those described for the polystyrene ball current in Figure 2 were observed for the snow currents: the crescent-shaped head and denser tail, the recirculation behind the head, and the raised nose.

[36] Figure 3 shows the evolution of one experiment at different points down the slope. This shows that the particles are initially concentrated in a smooth crescent at the front. As the current moves down the slope this front crescent spreads and flattens out and then becomes unstable. The spreading is to be expected, because there is no steady flow possible with a curved front where the pressure in the ambient fluid balances the hydrostatic spreading forces [*McElwaine*, 2005]. This instability as the flow front flattens is probably related to the well known, but poorly understood, lobe and cleft instability.

[37] In the following subsections, the video data of front velocity, flow height and lateral spreading are presented and discussed. However, we have not fitted this data because we

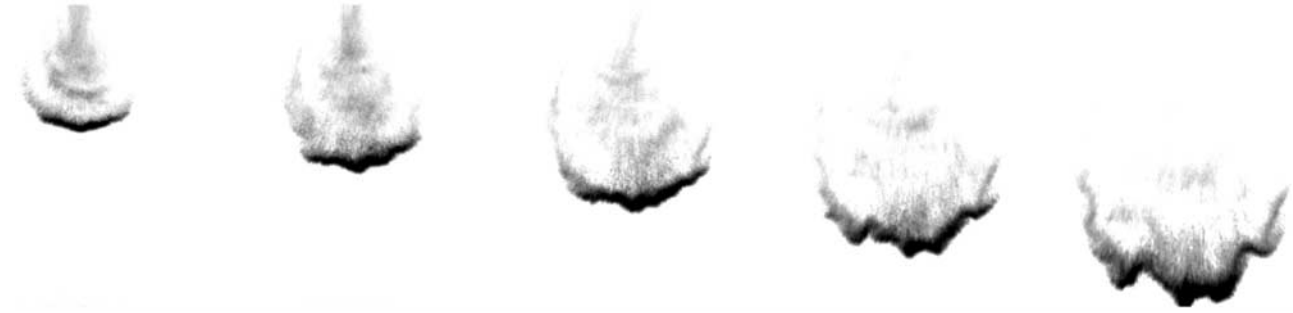

Figure 3. A 5l polystyrene current on a 51° slope showing front instability. The images are at three frame intervals, deinterlaced, and have an inverted color scheme with the background removed.

have no model for the three-dimensional flow. In particular, we have no solution for the lateral spread of the flows (section 4.3). We have scaled the data from the polystyrene ball experiments, informing us which parameters determine the flow dynamics. In the figures of front velocity (Figures 5, 6, and 7), flow height, and flow width, the marker shows the mean value at each slope angle and the error bar has length equal to the standard deviation from the mean for that slope angle.

4.1. Front Velocity

[38] Figure 4 shows the trajectory of two flow fronts, for a snow and a polystyrene ball current. The time origin $t = 0$ is the time when the flow front is level with the position of the pressure sensor. Since the gradient of the trajectory is the front velocity, the linear trajectory of the polystyrene ball currents shows that the flow reaches a steady front velocity along the length of the chute. In contrast, the snow-air current accelerates slightly along the length of the chute. The polystyrene currents have a change in velocity from the top to the bottom of the chute that is close to zero whereas the snow experiments show a difference of about 1.5 m s^{-1}. The main reason for the acceleration of the snow-air currents is that the snow particles have a higher fall velocity in air than the polystyrene balls. A current reaches dynamic equilibrium when the entrainment of air at the top surface matches the fall velocity of the particles. The snow currents thus take longer to reach this equilibrium than their polystyrene counterparts.

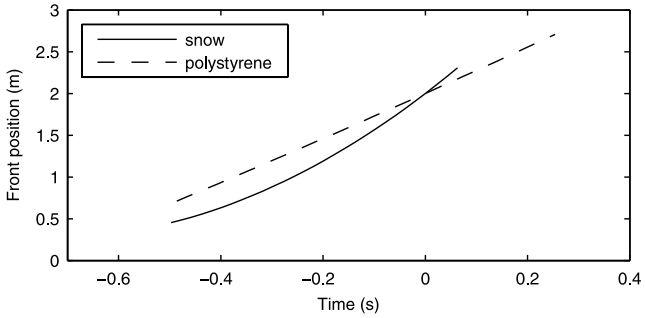

Figure 4. Typical front trajectories of a snow (solid line) and a polystyrene (dashed line) current. The time origin, $t = 0$, corresponds to the arrival of the current at the air pressure sensor.

[39] The final velocity raw data in Figure 5 (top and middle) show a large degree of scatter compared with any trend in the data. As found in the experiments of *Britter and Linden* [1980] for continuous, homogeneous gravity cur-

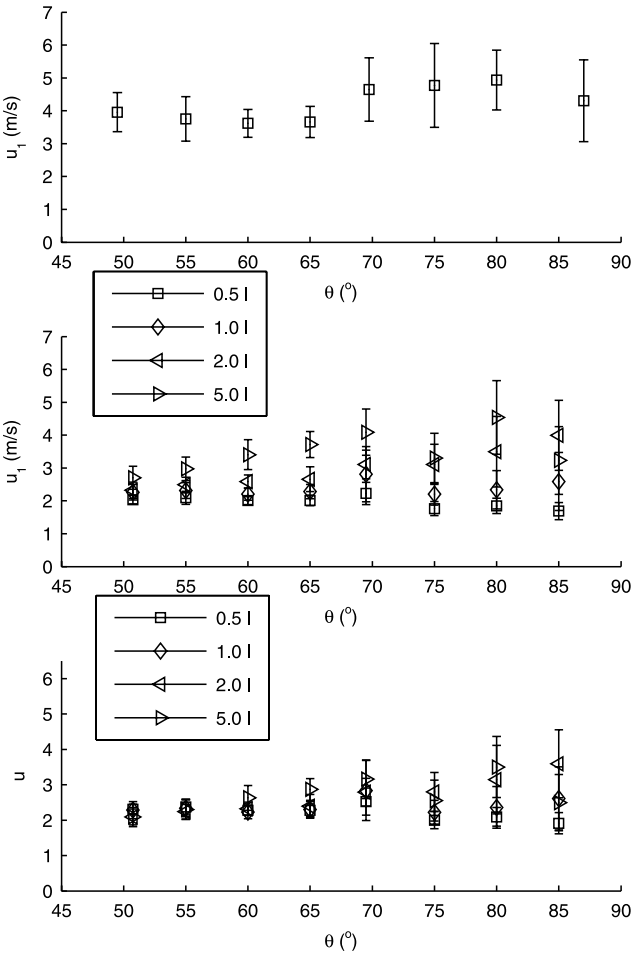

Figure 5. Final front velocity of the currents versus slope angle, θ. (top) Snow currents. (middle) Dimensional data from the polystyrene ball currents. (bottom) Nondimensionalized data from the polystyrene ball currents. At each slope angle the marker shows the mean velocity and the error bar has length equal to the standard deviation from the mean for that slope angle.

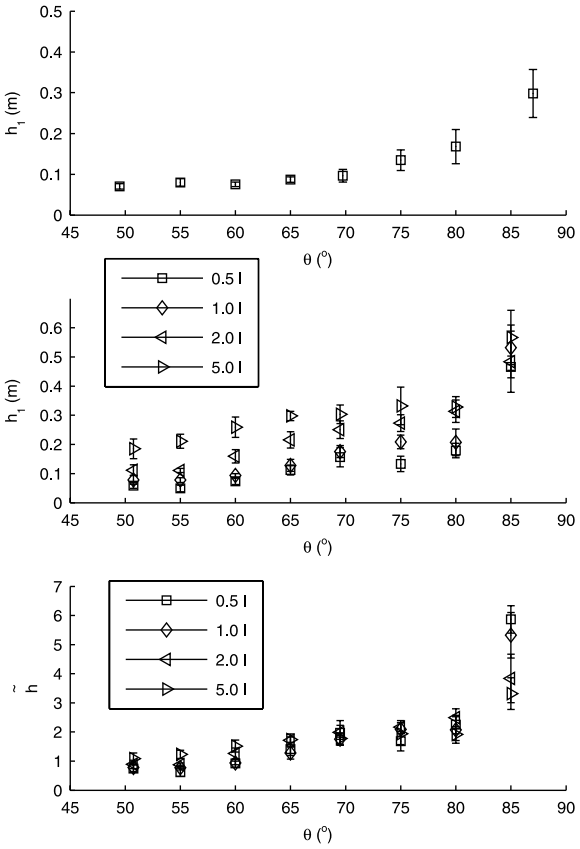

Figure 6. Final head height of the currents versus slope angle, θ. (top) Snow currents. (middle) Dimensional data from the polystyrene ball currents. (bottom) Nondimensionalized data from the polystyrene ball currents.

rents traveling on an incline, this indicates that the front velocity is independent of slope angle.

[40] For the polystyrene ball experiments the release volume, V, of particles was measured meaning the front velocity of these flows can be nondimensionalized. The length scale for the nondimensionalization is that which characterizes the release volume, $V^{\frac{1}{3}}$. The nondimensional front velocity is then

$$\tilde{u} = \frac{u}{V^{\frac{1}{6}} g^{\frac{1}{2}}}, \tag{7}$$

where g is the acceleration due to gravity ($g = 9.81$ m s^{-2}), shown for each slope angle in Figure 5 (bottom). Particularly at lower slope angles, where the initial conditions of the flows were better controlled (the particles have a smaller distance to fall between the drop tube and the chute surface), this scaling collapses the data.

4.2. Flow Height

[41] Current head heights at the end of the chute are shown at each slope angle in Figure 6. Scatter in the flow height measurements is small and the wide variation in initial conditions have been ''forgotten'' by the bottom of the chute. A clear trend can be seen, that flow height increases with increasing slope angle.

[42] For the polystyrene ball experiments, where the release volume was measured, the head heights have been scaled by the cube root of the release volume to give the nondimensional head height

$$\tilde{h} = \frac{h}{V^{\frac{1}{3}}}. \tag{8}$$

These scaled data are shown for each slope angle in Figure 6 (bottom). The good agreement of data from currents with different release volumes shows that for slope angles below 85° the data scales well with this release length scale. For a slope angle of 85° there is very large entrainment and it may be that our chute was too short for equilibrium to be reached at such steep inclinations.

4.3. Lateral Spreading

[43] The final widths of the snow and polystyrene currents are shown for each slope angle in Figure 7. At the bottom of the chute a clear trend can be seen, where the width of the current decreases with increasing slope angle. The current width has been nondimensionalized in the same way as the head height, scaled by the cube root of the release volume

$$\tilde{w} = \frac{w}{V^{\frac{1}{3}}}. \tag{9}$$

This scaling gives the nondimensional width for the polystyrene currents shown in Figure 7 (bottom). However,

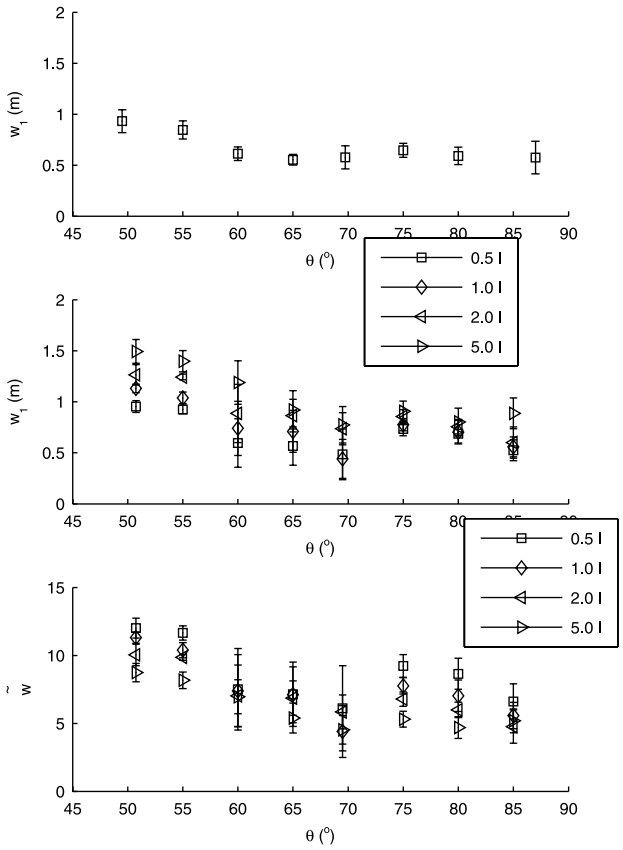

Figure 7. Final front lateral width of the currents versus slope angle, θ. (top) Snow currents. (middle) Dimensional data from the polystyrene ball currents. (bottom) Nondimensionalized data from the polystyrene ball currents.

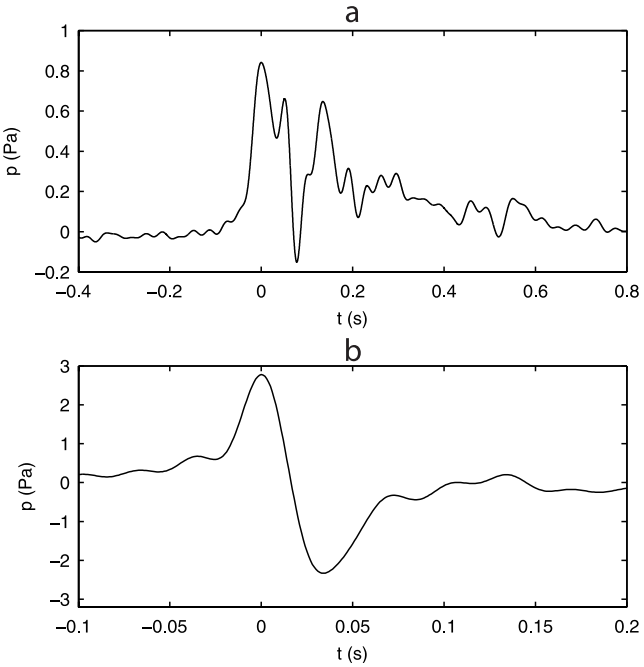

Figure 8. Air pressure in a snow-air suspension current at a slope angle of (a) 60°, where the current is only partially suspended, and (b) 70°, where the current is fully suspended. The time origin, $t = 0$, corresponds to the arrival of the current at the sensor.

this nondimensionalization does not scale the data effectively. This is because the initial length scale for the width is given by the diameter of the tube through which the balls were dropped. Eventually you would expect this to be forgotten, as demonstrated by the good collapse of the velocity and height data. To address this problem in future experiments, a release width that scales with $V^{\frac{1}{3}}$ should be used for each volume of particles.

5. Air Pressure

[44] Air pressure at a single point on the chute has been measured which gives us the temporal distribution of air pressure along each snow or polystyrene current. The air pressure measurements from all the experiments showed the same features. Typical signals from the snow-air experiments are shown in Figure 8. The positive pressure in front of the avalanche is that of a dipole [*McElwaine and Nishimura*, 2001; *McElwaine*, 2005], which is to leading order

$$\frac{1}{2}\rho_a u_d^2 \left(\frac{1}{1 - u_d t/r_d}\right)^3, \tag{10}$$

where r_d is the effective aerodynamic radius of the current, u_d its velocity, ρ_a is the air density, and the arrival of the current front at the sensor occurs at $t = 0$. The pressure then drops sharply over a short time, resulting in a period of very steep pressure gradient. This pressure gradient is akin to high shear stresses at the current front. On shallower slopes, where the current is not fully suspended, there is only a small negative pressure and little internal variations showing low internal deviations in air velocity from the mean (Figure 8a). At increasingly steeper slope angles the pressure drops rapidly to larger negative pressures directly behind the head (Figure 8b). The negative pressures can be several times larger than the maximum hydrostatic pressure, $\frac{1}{2}\rho u^2$, showing that internal velocities can substantially exceed the front velocity and confirming the hypothesis that the head dynamics are dominated by a large vortex [*Bozhinskiy and Losev*, 1998; *Grigoryan et al.*, 1982].

[45] This has very important implications for estimating the maximum bulk stresses avalanches can exert on structures. Large differences between the maximum and minimum pressure, occurring over a short time lead to stresses that cannot be predicted by a hydrostatic pressure assumption. Internal velocities that are substantially larger than the front velocity can also lead to individual lumps of dense snow that have much greater momentum, and thus much greater destructive force, than predictable from the front velocity only.

[46] The more controlled initial conditions for the polystyrene experiments meant that some of these pressure signals could be straightforwardly compared. Air pressure measurements from a series of experiments of the same release volume and at the same slope angle have been superimposed in Figure 9. The time origin has been set to the time of maximum pressure when the flow front reaches the sensor. The vortex behind the head is a surprisingly repeatable flow feature. We have also made air pressure measurements in powder snow avalanches in the field using a similar transducer mounted in a specially adapted housing in the avalanche path [*McElwaine and Turnbull*, 2004]. These pressure measurements show qualitatively similar structures to those from our chute currents. This supports the possibility for increased destructive forces due to the internal motion of the powder snow avalanche.

[47] In the case of the polystyrene ball currents, where the initial volume, V, of particles is known, there is a length scale $V^{\frac{1}{3}}$ from which a pressure scale $\rho_a V^{\frac{1}{3}} g$ is derived. Similarly a timescale is found, $V^{\frac{1}{6}}/g^{\frac{1}{2}}$. Our polystyrene ball air pressure versus time data are nondimensionalized with the above pressure and timescales. When scaled in this way using the release conditions, the air pressure distribution along the polystyrene ball currents is still dependent on the current release volume. This is because of the drop tube, the diameter of which is of a similar magnitude to the length $V^{\frac{1}{3}}$. Thus an additional length ratio is introduced into the flow, the drop tube diameter compared to the release volume

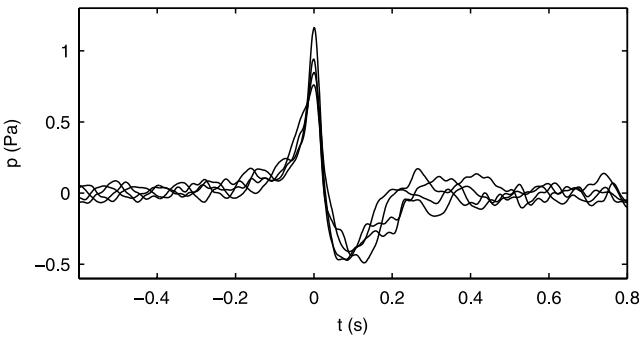

Figure 9. Air pressure measurements from five 0.5l polystyrene ball currents at a slope angle of 50.5°.

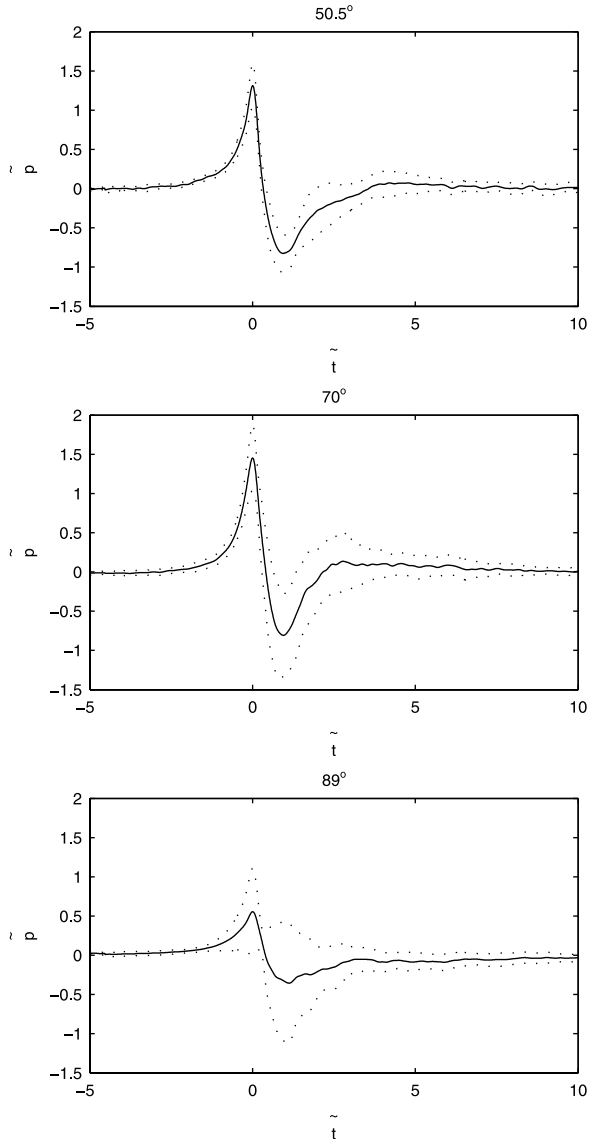

Figure 10. Scaled air pressure history from all of the polystyrene currents: ensemble mean (solid line), plus or minus the standard deviation from the ensemble mean (dashed line), at three different slope angles.

length scale. The air density, ρ_a at the altitude and temperature of the experiment (1650 m a. s. l. and around 0°C) is calculated from the 1976 standard atmosphere, and is close to 1 kg m^{-3}.

[48] The scaled polystyrene current air pressure data is shown in Figure 10. This is presented as an ensemble average of all the experiments at each slope angle, plus or minus the standard deviation from the mean. The lack of scatter up the minimum shows that the scaling works well up to this point, but the large amount of scatter in the tail shows that in the tail the flows are turbulent and not repeatable.

6. Comparison With Dynamic Theory for the Air Flow

[49] The nature of the pressure field on the center line through a gravity current is discussed in detail by *McElwaine* [2005]. The main result is that the pressure along the surface through the center of the flow is

$$p = \begin{cases} \frac{1}{2}\rho_a u^2 \frac{R^3}{(r+R)^3}\left(2 - \frac{R^3}{(r+R)^3}\right) & \text{OA } r/R > \lambda - 1 \\ \frac{1}{2}\rho_a u^2\left(1 - \kappa\frac{r}{R}\right) & \text{OA } r/R < \lambda - 1 \\ \frac{1}{2}\rho_a u^2\left(1 - \kappa\frac{r}{R}\right) + 2g(\rho - \rho_a) & \\ \quad \cdot r\sin\left(\frac{1}{2}\phi\right)\cos\left(\theta + \frac{1}{2}\phi\right) & \text{OB } r/R < O(\lambda - 1) \\ \text{unknown} & \text{OB } r/R = O(\lambda - 1) \\ \approx 0, \text{but turbulent fluctuations} & \text{BC.} \end{cases} \tag{11}$$

Ensuring continuity, solutions can be found to the cubic equations such that $\lambda \approx 1.39$ and $\kappa \approx 1.01$. ρ_a is the density of the air and ρ is the density of the current which is assumed constant. R is the effective length scale of the flow and $r = (t_0 - t)v$ is the distance from O, where t_0 is the time at which the front arrives at the sensor and v is the front speed. The positions and angles are defined in Figure 11. A strong result of this approach is that the front angle $\phi = 60°$.

[50] We would very much like to have measured the front angle accurately in our experiments to test this prediction, but the experimental errors were rather large, and though they are consistent with a 60° angle, they do not convincingly confirm it. Improved control over the initial conditions of the flow in future experiments may help.

[51] It does not seem likely that there can be any simple, general theory that covers the latter part of the current (marked as unknown in equation (11)) for all slope angles since in general the flow will be turbulent with many eddies. The wake of the current may also be turbulent, and the pressure may fluctuate significantly about zero. In some cases however, if the whole current is essentially one large vortex, the approximation on OB $r/R < O(\lambda - 1)$ can be continued linearly to E and the pressure along EB will also be linear.

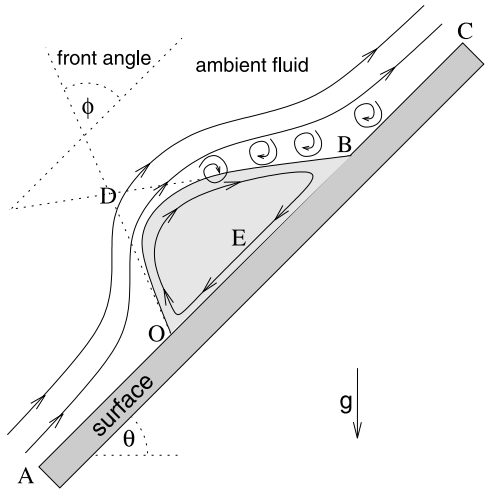

Figure 11. Schematic of a current on a slope.

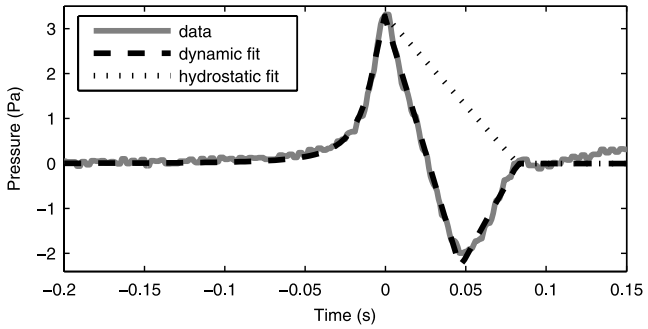

Figure 12. Comparison of air pressure data from a snow experiment on a 70° slope with the dynamic theory and a hydrostatic theory.

[52] The parameters to be fitted are R and u from equation (11) the arrival time $t_0 \approx 0.14$ s (point O), the pressure minimum and the time at which it occurs $t_1 \approx 0.19$ s (point E), and the time at which the pressure returns to zero $t_2 \approx 0.22$ s (point B). These were found using a least squares fitting procedure and the excellent agreement is shown in Figure 12. The implied density ρ can then be found using equation (11). The fitted pressure distribution gave the speed $u = 2.6$ m s^{-1}, the aerodynamic flow radius $R = 0.05$ m and the density of the flow $\rho = 13$ kg m^{-3}. The speed and size are in agreement with the video observations. The density suggests a volume fraction of around 2% which is reasonable, but there was no independent measurement of this. The other curve in Figure 12 shows a fit to a hydrostatic model where the internal velocities are zero so the pressure decreases linearly between t_0 and t_2, which is assumed to correspond to the end of the avalanche. This model suggests the internal density is $\rho = 2.7$ kg m^{-3}. The total disagreement with a hydrostatic model is striking. It is remarkable that the pressure inside the flow is so well matched by two linear pressure profiles. This is the result of the large eddy the center of which corresponds to the pressure minimum at t_1. The linear fit between t_1 and t_2 is presumably the second half of the eddy.

[53] Few of the pressure signals however fit as well as this figure would suggest. Most flows have a more complicated structures and do not consist of a single, cleanly structured eddy. Fits to some of the experiments are shown in Figures 13 and 14, where there is agreement, but less striking. In particular there is a distinct curvature in both the falling and rising signal within the current. The wide

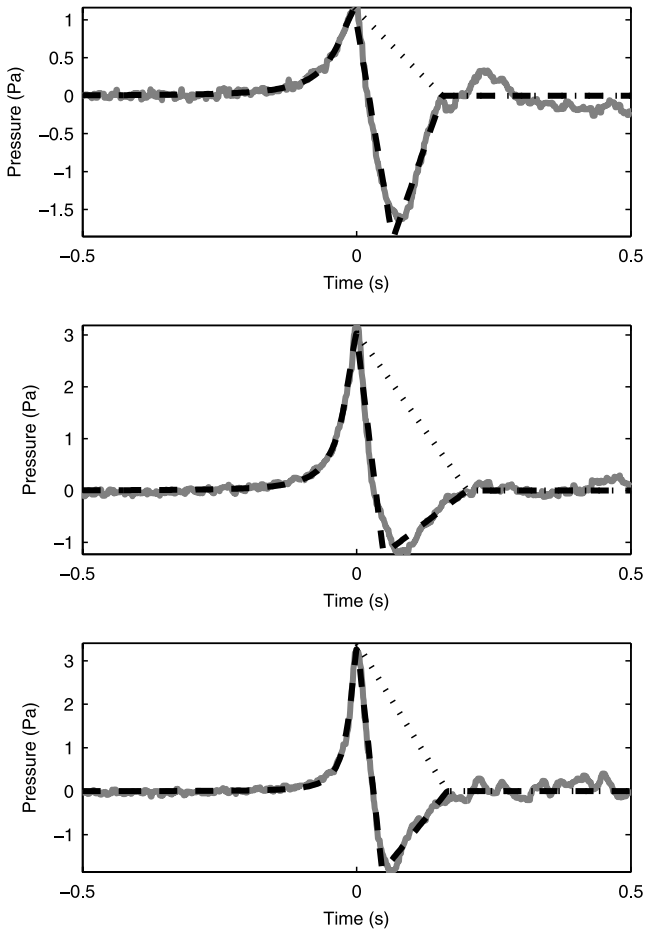

Figure 13. Pressure histories of typical individual snow currents (grey line), dynamic fit (dashed line), and hydrostatic approximation (dotted line).

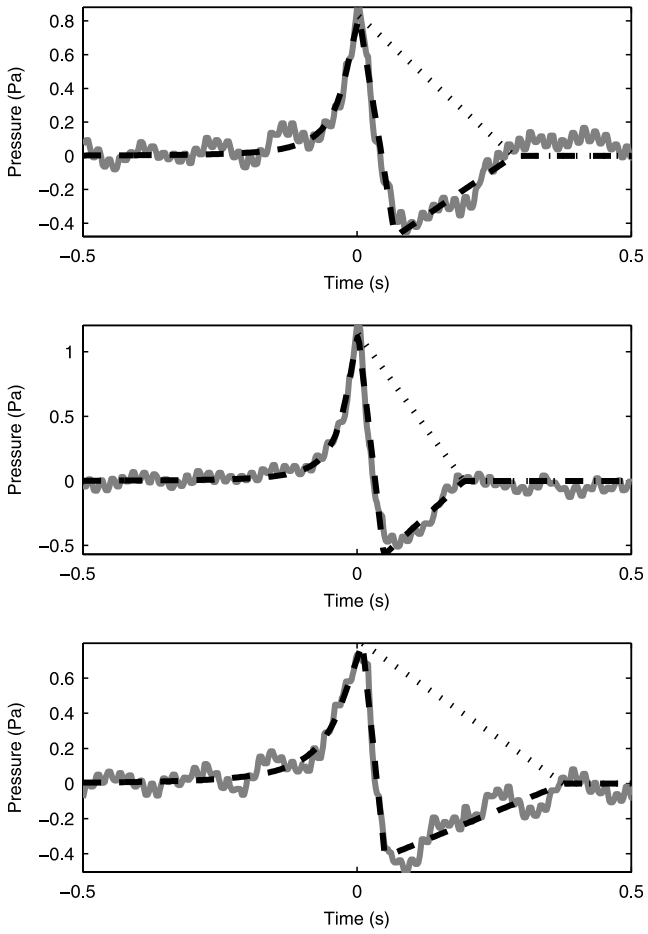

Figure 14. Pressure histories of typical individual polystyrene currents (grey line), dynamic fit (dashed line), and hydrostatic approximation (dotted line).

variation in the latter half of the pressure signals has been shown in Figure 10.

7. Conclusions

[54] High density ratio, non-Boussinesq, self-igniting, particulate suspension currents in air have been generated in the laboratory in a systematic and repeatable way. These currents have many of the correct similarity criteria, including the Richardson number and bulk density, to physically model powder snow avalanches. Though the experiments are not perfect, and the empirical scatter is too large to draw many quantitative conclusions, we have shown that polystyrene-air and snow-air currents behave in qualitatively the same way. We have shown a good agreement with theory of the structure of the air flow, both internal and external to the current, and demonstrated how dense flows and suspended currents give qualitatively different results. This may have important implications for designing structures to resist avalanches since we have shown that there can be coherent, internal flow fields with velocities several times that of the front velocity, leading to much larger destructive forces than might otherwise have been expected. However, because our experiments do not have similar Reynolds numbers or Stokes numbers straightforward conclusions for practical applications cannot be drawn.

[55] **Acknowledgments.** We would like to thank Marcia Phillips for help measuring the snow properties and logistical support, Perry Bartelt for supporting the project, and Christophe Ancey for his constructive comments. The project and authors received support from the EU (SATSIE EVG1-CT2002-00059), the Isaac Newton Trust, the Swiss National Science foundation, the Royal Society and EPSRC (GR/TO2416101).

References

Ancey, C. (2004), Powder-snow avalanches: Approximation as non-Boussinesq clouds with a Richardson number–dependent entrainment function, *J. Geophys. Res.*, *109*, F01005, doi:10.1029/2003JF000052.

Ancey, C. (2007), Plasticity and geophysical flows: A review, *J. Non-Newtonian Fluid Mech.*, *142*, 4–35, doi:10.1016/j.jnnfm.2006.05.005.

Assier Rzadkiewicz, S., C. Mariotti, and P. Heinrich (1997), Numerical simulation of submarine landslides and their hydraulic effects, *J. Waterw. Port Coastal Ocean Eng.*, *123*(4), 149–157.

Batchelor, G. (1967), *An Introduction to Fluid Dynamics*, Cambridge Univ. Press, New York.

Batchelor, G. (1989), A brief guide to two-phase flow, in *Theoretical and Applied Mechanics*, edited by P. Germain, J. Piau, and D. Caillerie, pp. 27–41, Elsevier Sci., New York.

Beghin, P., and G. Brugnot (1983), Contribution of the theoretical and experimental results to powder-snow avalanche dynamics, *Cold Reg. Sci. Technol.*, *8*, 67–73.

Beghin, P., and X. Olagne (1991), Experimental and theoretical study of the dynamics of powder snow avalanches, *Cold Reg. Sci. Technol.*, *19*, 317–326.

Beghin, P., E. Hopfinger, and R. Britter (1981), Gravitational convection from instantaneous sources on inclined boundaries, *J. Fluid Mech.*, *107*, 407–422.

Boussinesq, J. (1903), *Théorie Analytique de la Chaleur* (in French), vol. 2, Gathier-Villars, Paris.

Bozhinskiy, A., and L. Sukhanov (1998), Physical modelling of avalanches using an aerosol cloud of powder material, *Ann. Glaciol.*, *26*, 242–394.

Bozhinskiy, N., and K. Losev (1998), *Fundamentals of Avalanche Science*, translated from Russian by C. E. Bartelt, Eidg. Inst. für Schnee- und Lawinenforsch., Davos, Switzerland.

Britter, R., and P. Linden (1980), The motion of the front of a gravity current travelling down an incline, *J. Fluid Mech.*, *99*, 531–543.

Dufour, F., et al. (1999), Vallée de la Sionne winter report, technical report, Eidg. Inst. für Schnee- und Lawinenforsch., Davos, Switzerland.

Dufour, F., et al. (2000), Vallée de la Sionne winter report, technical report, Eidg. Inst. für Schnee- und Lawinenforsch., Davos, Switzerland.

Dufour, F., et al. (2001), Vallée de la Sionne winter report, technical report, Eidg. Inst. für Schnee- und Lawinenforsch., Davos, Switzerland.

Dufour, F., et al. (2002), Vallée de la Sionne winter report, technical report, Eidg. Inst. für Schnee- und Lawinenforsch., Davos, Switzerland.

Dufour, F., et al. (2003), Vallée de la Sionne winter report, technical report, Eidg. Inst. für Schnee- und Lawinenforsch., Davos, Switzerland.

Dufour, F., et al. (2004), Vallée de la Sionne winter report, technical report, Eidg. Inst. für Schnee- und Lawinenforsch., Davos, Switzerland.

Dufour, F., et al. (2005), Vallée de la Sionne winter report, technical report, Eidg. Inst. für Schnee- und Lawinenforsch., Davos, Switzerland.

Ellison, T., and J. Turner (1959), Turbulent entrainment in stratified flows, *J. Fluid Mech.*, *6*, 423–448.

Grigoryan, S., N. Urumbayev, and I. Nekrasov (1982), Experimental'noye issledovaniye lavinnoy vozdushnoy volny [Experimental studies of an avalanche wind], *Mater. Glyatsiol. Issl.*, *44*, 87–94.

Hampton, M. (1972), The role of sub-aqueous debris flow in generating turbidity currents, *J. Sediment. Petrol.*, *42*, 775–793.

Hermann, F., J. Hermann, and K. Hutter (1987), Laboratory experiments on the dynamics of powder snow avalanches, in *International Symposium on Avalanche Formation, Movement and Effects, Proceedings of the Davos Symposium, Sept. 1986*, *IAHS-Publ.*, *162*, 431–439.

Hopfinger, E., and J. Tochon-Danguy (1977), A model study of powder snow avalanches, *J. Glaciol.*, *81*, 343–356.

Issler, D. (1998), Modelling of snow entrainment and deposition in powder-snow avalanches, *Ann. Glaciol.*, *26*, 253–258.

Margreth, S. (2000), Gutachten betreffend unglückslawinen in Galtür vom 23.2.1999 und in Valzur vom 24.2.1999, SLF Gutachten G2000 (in German), *Rep. 12*, pp. 15–18, Swiss Fed. Inst. for Snow and Avalanche Res. (SLF), Davos Dorf, Switzerland.

McElwaine, J. (2001), Image analysis for avalanches, paper presented at International Seminar on Snow Avalanches Experimental Sites, French Assoc. for Snow and Avalanche Study (ANENA), Grenoble, France.

McElwaine, J. (2005), Rotational flow in gravity current heads, *Philos. Trans. R. Soc.*, *363*, 1603–1623, doi:10.1098/rsta.2005.1597.

McElwaine, J., and B. Turnbull (2004), Air pressure data from the Vallée de la Sionne avalanches of 2004, technical report, Eidg. Inst. für Schnee- und Lawinenforsch., Davos, Switzerland.

McElwaine, J. N., and K. Nishimura (2001), Ping-pong ball avalanche experiments, in *Particulate Gravity Currents*, *IAS Spec. Publ.*, vol. 31, edited by W. D. McCaffrey, B. C. Kneller, and J. Peakall, pp. 135–148, Blackwell Sci., Malden, Mass.

Nishimura, K. (1990), Studies on the fluidized snow dynamics, in *Contrib. Inst. Low Temp. Sci. 37A*, 55 pp., Hokkaido Univ., Sapporo, Japan.

Nishimura, K., F. Sandersen, K. Kristensen, and K. Lied (1995), Measurements of powder snow avalanche—Nature, *Surv. Geophys.*, *16*, 649–660.

Nishimura, K., S. Keller, J. McElwaine, and Y. Nohguchi (1998), Ping-pong ball avalanche at a ski jump, *Granular Matter*, *1*(2), 51–56.

Parker, G. (1982), Conditions for the ignition of catastrophically erosive turbidity currents, *Mar. Geol.*, *46*, 307–327.

Parker, G., Y. Fukushima, and H. Pantin (1986), Self-accelerating turbidity currents, *J. Fluid Mech.*, *171*, 145–181.

Simpson, J. (1997), *Gravity Currents in the Environment and the Laboratory*, Cambridge Univ. Press, New York.

Tochon-Danguy, J., and E. Hopfinger (1974), Simulation of the dynamics of powder avalanches, in *Proceedings of the Grindlewald Symposium*, *IAHS-AISH Publ.*, *114*, 369–380.

Turnbull, B., and J. N. McElwaine (2007), A comparison of powder snow avalanches at Vallée de la Sionne with plume theories, *J. Glaciol.*, *53*, 30–40.

Turnbull, B., J. N. McElwaine, and C. J. Ancey (2007), The Kulikovskiy-Sveshnikova-Beghin model of powder snow avalanches: Development and application, *J. Geophys. Res.*, *112*, F01004, doi:10.1029/2006JF000489.

Turner, J. (1973), *Buoyancy Effects in Fluids*, Cambridge Univ. Press, New York.

J. N. McElwaine, Department of Applied Mathematics and Theoretical Physics, University of Cambridge, Wilberforce Road, Cambridge CB3 0WA, UK. (jnm11@cam.ac.uk)

B. Turnbull, Mechanical and Aerospace Engineering, Cornell University, 146 Upson Hall, Ithaca, NY 14853, USA. (abt43@cornell.edu)